Int. J. Electrochem. Sci., 9 **(2014)** 6880 - 6895

International Journal of
ELECTROCHEMICAL
SCIENCE
www.electrochemsci.org

Experimental and Theoretical Investigation of 1-hydroxybenzotriazole as a Corrosion Inhibitor for Mild Steel in Sulfuric Acid Medium

Ruxi Chen[1,*], *Lei Guo*[2], *Shenying Xu*[1, 2]

[1]School of Chemistry and Chemical Engineering, Yibin University, Yinbin 644000, P. R. China
[2] School of Chemistry and Chemical Engineering, Chongqing University, Chongqing 400044, P. R. China
[*]E-mail: crfyibin@163.com

Received: 3 August 2014 / *Accepted:* 11 September 2014 / *Published:* 29 September 2014

The inhibition effect of 1-hydroxybenzotriazole (HOBT) on the corrosion of mild steel in 0.1 mol L^{-1} H_2SO_4 solution was investigated using weight loss, electrochemical measurement and SEM observation. The polarization curves indicated that HOBT behaved as a mixed-type inhibitor while the Nyquist plots revealed that the corrosion was a charge transfer controlled process. Moreover, the absorption of HOBT was found to obey the Langmuir adsorption isotherm. The free energy of adsorption (ΔG_{ads}) was found to be −30.54 kJ mol^{-1} and this value indicated that the adsorption was mainly chemisorption. The reactive ability, as well as the gas-phase adsorption of standalone HOBT molecule on perfect Fe(110) surface has been studied and characterized by means of density functional theory calculations.

Keywords: 1-hydroxybenzotriazole, Electrochemical investigation, Weight loss measurement, Corrosion inhibitor, Mild steel, Quantum chemical

1. INTRODUCTION

Corrosion inhibitors have been widely studied in many industries to reduce the corrosion rate of metal materials in contact with aggressive medium [1-3]. Most well-known acid inhibitors are organic compounds with π-electrons and functional groups containing heteroatoms which can donate lone-pair electrons [4, 5]. The efficiency of these molecules mainly depends on their abilities to be adsorbed on the metal surface with the polar groups acting as the reactive centers. Among them, Nitrogen-containing compounds of the triazole-type were confirmed as effective inhibitors for many metals [6-8] and alloys [9] due to the presence of three nitrogen atoms in an aromatic ring. For

example, benzotriazole is an effective inhibitor for Cu [10-12] and Fe [13, 14]. HOBT, benzotriazole derivative with an oxygen-containing substituent, is currently the most frequently used activating agent for the carboxyl group of amino acids. Its molecular structure provides a theoretical consideration for its inhibiting performance study. To facilitate the presentation the structure of HOBT along with the numbering of atoms is presented in Fig. 1.

Moreover, clarification of the interaction between inhibitor molecules and surface metal atoms at the molecular level is important in terms of finding new and effective inhibitors. Classic molecular dynamics simulation is one approach to obtain such data, but can be limited by the reliability of the force-field used. Quantum chemical calculations are proved to be a very powerful tool for studying the inhibition mechanism [4, 15-17]. It is feasible to model at a high level of theory the hard/soft matter interfaces, including covalent, donor–acceptor, H-bonding and van der Waals types of interactions. Recently, few studies have appeared in the literature, for cluster systems or slabs where dispersion forces are taken into account in a DFT approach when studying organic molecules adsorbed on inorganic surfaces using specific functional or other methods where long-range interactions are reachable [18-20].

Hence, the objective of the present work was to first investigate the effect of HOBT on the corrosion of mild steel corrosion in 0.1 M H_2SO_4 solution using experimental method and to subsequently clarify its interaction with the Fe(110) surface by density functional theory including dispersive forces (DFT-D) calculations.

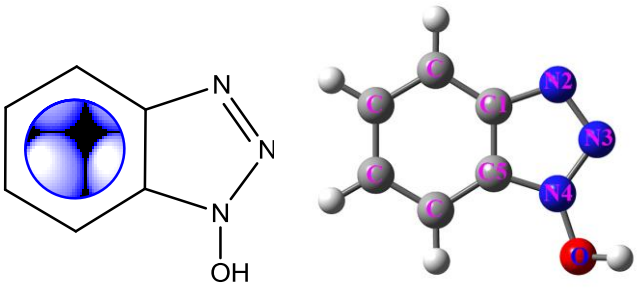

(a) (b)

Figure 1. (a) Lewis structure and (b) ball and stick model of HOBT. Numbering of atoms is also indicated.

2. EXPERIMENTAL

2.1. Materials and sample preparation

The corrosion tests were performed on mild steel of the following composition: 0.17% C, 0.26% Si, 0.47% Mn, 0.017% S, and the remained is Fe. HOBT was dissolved in 0.1 M H_2SO_4 at different concentrations (from 50 mg L^{-1} to 650 mg L^{-1}). The solution in the absence of HOBT was taken as blank for comparison.

A bulk of mild steel was mechanically cut into 3.0 cm × 2.0 cm × 1.0 cm dimensions for weight loss measurement, and 1.0 cm × 1.0 cm × 1.0 cm dimensions for surface analysis, respectively. For electrochemical tests, the specimens were embedded in epoxy resin with a geometrical surface area of 1.00 cm^2 exposed to the corrosive medium. The surfaces of all the specimens were polished successively with SiC paper from grade 400 to 1200, then were washed with distilled water, degreased ultrasonically in acetone, dried at room temperature and finally placed in a desiccator.

2.2. Electrochemical test

The electrochemical studies were carried out with CHI604D electrochemical workstation (Shanghai Chenhua CO., LTD) in a traditional three-electrode cell at 298K. A platinum sheet and a saturated calomel electrode (SCE) were used as auxiliary and reference electrode, respectively. All potentials were referred to SCE reference electrode. Electrochemical impedance spectroscopy (EIS) measurements were carried out at the open circuit potential (E_{OCP}). The alternating current frequency range extended from 10^{-1} Hz to 10^5 Hz with a 5 mV amplitude. Then the impedance data were analyzed and fitted. The potentiodynamic polarization curves were obtained from –250 mV to + 250 mV versus E_{OCP} with a sweep rate of 2.0 mV s^{-1}. All experiments were performed under atmospheric conditions. Each experiment was repeated at least three times to check the reproducibility.

2.3. Weight loss experiment

Polished and dried steel specimens were immersed in 500 mL 0.1 M H_2SO_4 solutions for 6 h in the absence and presence of various concentrations of HOBT at 298 K. The temperature was controlled thermostatically using an aqueous thermostat. The initial weight of each specimen was recorded before immersion using an analytical balance of 0.1 mg accuracy. After the immersion, the specimens were subjected to ultrasonic cleaning, dried and reweighed. Duplicate experiments were performed in each case for the same condition and the mean value of the corrosion rate was determined.

2.4. SEM analysis

The surface morphology of specimens after immersion in 0.1 M H_2SO_4 in the absence and presence of HOBT was performed on a KYKY2800B scanning electron microscope. The accelerating voltage was 20 kV.

2.5. Computational details

Firstly, the DFT calculations for the HOBT molecule were accomplished by means of the Gaussian 09 program to analyze the structural and electronic parameters; the structures were fully optimized, and vibrational analyses were carried out to verify that the optimized geometries

corresponded to minimum global energy. The popular Becke's three-parameter hybrid functional (B3LYP) [21] method in combination with the 6-311++G(d,p) basis set has been chosen.

Furthermore, the supercell approach was also employed to describe the interactions between the inhibitor and Fe(110) surface in a simulation box (12.4 Å × 12.4 Å × 24.1 Å) with periodic boundary conditions. The Fe(110) was first built and relaxed. The surface area was increased and its periodicity was changed by constructing a 3-layer 5 × 5 supercell, with a vacuum slab of thickness 20 Å. The three bottom layers of the slab were kept frozen to the bulk positions, while all other degrees of freedom were relaxed. Spin-polarized DFT calculations were performed in the framework of generalized gradient approximation (GGA) of Perdew-Burke-Ernzerhof (PBE) [22] using the linear combination of atomic orbitals (LCAO) method with DFT-based semicore pseudopotentials (DSPPs) [23] core treatment as implemented in the DMol^3 code of the Materials Studio 6.0 software (Accelrys Inc., San Diego, CA, USA) [24]. The valence electron functions were expanded into a set of numerical atomic orbits by a double-numerical basis with polarization functions (DNP) [25]. Brillouin-zone integrations were performed using 3 × 3 × 1 *k*-point grid which was generated automatically using the Monkhorst–Pack method. The tolerances of energy, gradient, and displacement convergence were 1 × 10^{-5} Ha, 2 × 10^{-3} Ha Å^{-1}, and 5 × 10^{-3} Å respectively. The lattice constant of bulk bcc Fe was calculated to be 2.89 Å, in good agreement with previous theoretical [26] and experimental work [27]. At this lattice constant, the total magnetization was found to be 2.60 μ_B per atom once again in good agreement with previous work [28, 29]. The total magnetic moment per atom of the 3-layer slab was calculated to be 2.72 μ_B in ferromagnetic order.

To explore the influence of van der Waals (vdW) forces on the geometry, we performed systematically parallel calculations in the DFT and DFT-D schemes. The DMol^3 code allows the estimation of the dispersion forces in the calculations using Grimme's method [30]. Quantitative appraisal of the interaction was achieved by calculating the adsorption energy (E_{ads}) using formula:

$$E_{ads} = E_{tot}^{surf+ad} - \left(E_{tot}^{surf} + E_{tot}^{ad}\right) \quad (1)$$

where the first term is the total energy of the full system (surface + adsorbate), the second term is the energy of the bare Fe(110) surface and the last term is the energy of the gas-phase molecule. Based on this definition, a negative value of E_{ads} corresponds to a stable adsorption structure. In order to investigate the changes of electronic structures when the adsorbates chemisorbed on the Fe(110) surface, deformation charge density $\Delta\rho(\mathbf{r})$ was calculated. It is defined as

$$\Delta\rho(\mathbf{r}) = \rho_{total}(\mathbf{r}) - \sum \rho_{atom}(\mathbf{r}) \quad (2)$$

where $\rho_{total}(\mathbf{r})$ and $\rho_{atom}(\mathbf{r})$ are electron density of the adsorbate–surface adsorption system and individual isolated atom, respectively.

3. RESULTS AND DISCUSSION

3.1. Potentiodynamic polarization measurements

The representative polarization curves for mild steel in 0.1 M H_2SO_4 solution with HOBT at different concentrations was shown in Fig. 2. In order to obtain information about the kinetics of the

corrosion, some electrochemical parameters, *i.e.*, corrosion potential (E_{corr}), corrosion current density (i_{corr}), anodic and cathodic tafel slopes (β_a, β_c) obtained from the polarization measurements were listed in Table 1. The inhibition efficiency (η_p) was calculated using the following equation:

$$\eta_p = \frac{i_{corr(0)} - i_{corr(inh)}}{i_{corr(0)}} \times 100 \qquad (3)$$

where $i_{corr(0)}$ and $i_{corr(inh)}$ represent corrosion current density values without and with inhibitor, respectively. The i_{corr} values were determined by the extrapolation of the linear portions of the tafel curves to the corresponding corrosion potentials.

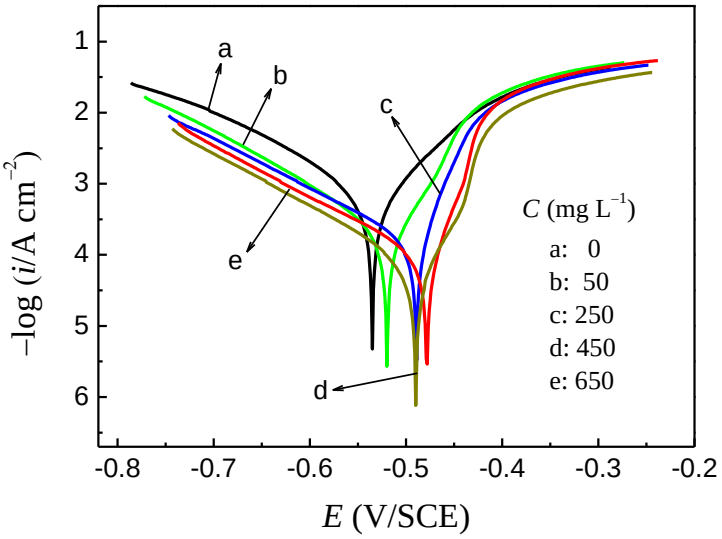

Figure 2. Polarization curves for mild steel in 0.1 M H_2SO_4 with different concentrations of HOBT.

Inspection of Fig. 2 shows that the addition of HOBT has an inhibitive effect in the both anodic and cathodic parts of the polarization curves and shifts both the anodic and cathodic curves to lower current densities. The reduction in i_{corr} is pronounced more and more with the increasing inhibitor concentration. It has been observed that 450 mg L^{-1} of HOBT serves as an optimum concentration that exhibit higher efficiency of corrosion inhibition. The increased inhibition efficiency with the inhibitor concentration indicates that the tested organic compound acts by adsorbing on the mild steel surface. The presence of HOBT in 0.1 M H_2SO_4 solution shifts the corrosion potential slightly towards more positive potentials with respect to the corrosion potential observed in the unhibited solution. The largest displacement of E_{corr} was about 59 mV (< 85 mV), which indicates that HOBT might act as a mixed-type inhibitor with predominant anodic effectiveness [31]. The cathodic branch of polarization curves was given rise to parallel lines. This shows that the addition of HOBT to the 0.1 M H_2SO_4 solution does not change the cathodic hydrogen evolution mechanism and the decrease of H^+ ions on the surface of mild steel take place mainly through a charge transfer mechanism [32]. The inhibition effect of HOBT may be caused by the simple blocking effect, namely the reduction of reaction area on the corroding surface.

Table 1. Electrochemical polarization parameters for mild steel in 0.1 M H_2SO_4 solution containing various concentrations of HOBT

C (mg L^{-1})	E_{corr} (mV)	i_{corr} (μA cm^{-2})	β_c (mV dec^{-1})	β_a (mV dec^{-1})	η_p
0	–535	654.7	7.634	11.05	/
50	–520	272.4	8.220	19.09	58.39
250	–489	147.7	6.823	26.78	77.44
450	–490	49.61	7.520	24.71	92.42
650	–478	74.87	6.693	30.39	88.56
850	–476	147.9	6.466	27.90	77.41

3.2. Electrochemical impedance spectroscopy (EIS)

Nyquist impedance diagrams of mild steel in 0.1 M H_2SO_4 solution in the absence and presence of various concentrations of HOBT are shown in Fig. 3. It can be observed that all impedance spectra show a single depressed capacitive loop in the high frequency range, which is related to charge transfer of the corrosion process. The capacitive loops are not perfect semicircles which can be attributed to the frequency dispersion effect as a result of the roughness and inhomogeneous of electrode surface [33]. The standard Randles' circuit model was used and is shown in Fig. 4a. Besides, inductive loops were observed in the low frequency range at high concentrations. reaction. Their presence might be attributed to the relaxation process obtained by adsorption species as H^+_{ads} and SO^{2-}_4 on the electrode surface [34]. It might be also attributed to the re-dissolution of the passivated surface at low frequencies [35]. In this case, the related electrochemical equivalent circuit model is shown in Fig. 4b. The solution resistance Rs, charge-transfer resistance R_{ct}, constant phase element (CPE) and inductive elements of L and R_L were fitted, and their values are listed in Table 2. CPE has the value of the frequency-distributed double-layer capacitance. The impedance function of the CPE is represented by the expression

$$Z_{CPE} = Y_0^{-1}(j\omega)^{-n} \qquad (4)$$

where Y_0 is a proportionality coefficient, ω is the angular frequency (in rad s^{-1}) and $j^2 = -1$ is the imaginary number, n is the exponent related to the phase shift and can be used as a measure of the surface inhomogeneity[36]. While $n = 0$, the CPE represents a pure resistor, for $n = -1$ an inductor and for $n = +1$, a pure capacitor[37]. The values of the double layer capacitance (C_{dl}) and inhibition efficiency (η_R) are calculated as follow:

$$C_{dl} = \frac{Y_0\omega^{n-1}}{\sin(n\pi/2)} \qquad (5)$$

$$\eta_R = \frac{R_{ct(inh)} - R_{ct(0)}}{R_{ct(inh)}} \times 100 \qquad (6)$$

where $R_{ct(0)}$ and $R_{ct(inh)}$ are the charge transfer resistance in the absence and presence of the inhibitor, respectively.

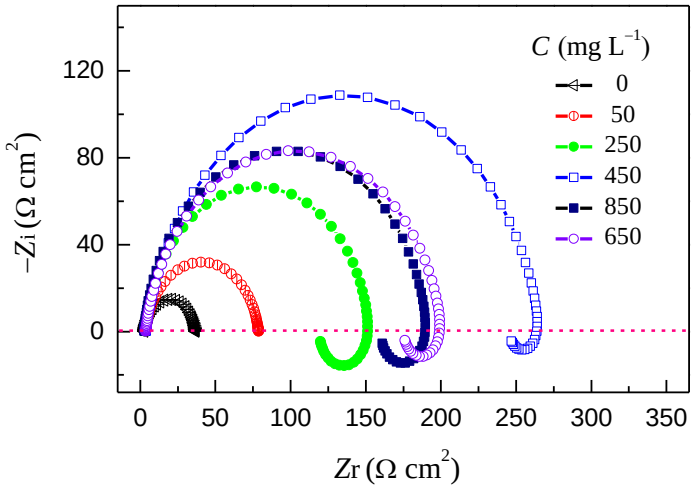

Figure 3. Nyquist diagrams for mild steel in 0.1 M H_2SO_4 containing different concentrations of HOBT

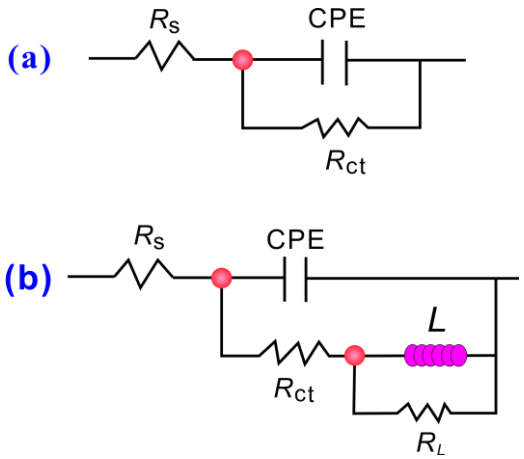

Figure 4. Equivalent circuits used to fit the EIS data of mild steel in 0.1 M H_2SO_4 + *x* mg L^{-1} inhibitor without (a) and with (b) inductive loop.

It can be seen from Table 2 that the solution resistance is very small and thus can be negligible. The R_{ct} values increased with the increasing of HOBT concentration which indicated the insulated adsorption layer's formation. When the concentration of HOBT was 450 mg L^{-1}, the capacitive reactance arc radius reached the largest. After that, when we continued increasing the concentration of the HOBT, the capacitive reactance arc radius decreased sharply, then the corrosion inhibition efficiency decreased. This is basically consistent with previous tafel analysis. The addition of HOBT provides lower Y_0 values, probably as a consequence of replacement of water molecules by inhibitor at the electrode surface. Also the inhibitor molecules may reduce the capacitance by increasing the double layer thickness according to the well known Helmholtz model [38]:

$$C_{dl} = \frac{\varepsilon^0 \varepsilon}{\delta} A \qquad (7)$$

where δ is the thickness of the protective layer, ε^0 is the permittivity of the air, ε is the local dielectric constant and A is the electrode surface area. The increase in thickness of the double layer was confirmed by the decrease in double layer capacitance values, which in turn justify that the inhibitor reduces the metal dissolution by effective adsorption.

Table 2. Fitted parameters of the equivalent electron circuit

C (mg L^{-1})	R_s (Ω cm^2)	CPE		R_{ct} (Ω cm^2)	R_L (Ω cm^2)	L (H cm^2)	η_R
		Y_0 (μF cm^{-2})	n				
0	2.690	216.4	0.9093	34.12	/	/	/
50	3.545	170.3	0.8954	75.26	/	/	54.66
250	3.401	104.2	0.9271	115.9	33.54	64.45	70.56
450	3.825	104.1	0.8796	242.0	21.13	71.92	85.91
650	2.633	90.9	0.9198	157.3	31.43	78.32	78.31
1050	3.816	122.1	0.8947	144.2	38.32	21.79	76.34

3.3. Weight loss test and the Adsorption behavior

The corrosion rates (v) of steel specimens after 6 h of exposure to 0.1 M H_2SO_4 solution with and without the addition of different concentrations of HOBT were calculated, and the values are summarized in Table 3. Corrosion rate v and the corrosion inhibition efficiency (η_w) were obtained by the following formulas:

$$v = \frac{\Delta W}{S \cdot t} \quad (8)$$

$$\eta_w = \frac{v_0 - v_i}{v_0} \times 100 \quad (9)$$

where ΔW is the average weight loss (mg), S is the surface area of specimens (cm^2), t is the immersion time (h), v_0 and v_i represent the corrosion rate in the absence and presence of HOBT, respectively.

Table 3. Weight loss data of mild steel in 0.1 M H_2SO_4 solution with different concentrations of HOBT for 6h

C (mg L^{-1})	v (mg cm^{-2} h^{-1})	Surface coverage (θ)	η_w
0	1.0090	/	/
50	0.5339	0.4708	47.08
250	0.2795	0.7223	72.23
450	0.1272	0.8734	87.34
650	0.1572	0.8442	84.42
850	0.2050	0.7968	79.68

From Table 3, we can see that, when the concentration of HOBT was less than 450 mg L^{-1}, v decreased while the inhibition efficiency increased with the increasing concentration. And the corrosion rate reached to the minimum at 450 mg L^{-1}, but the inhibition efficiency reached to maximum. After that, continuing increasing the inhibitor concentration, the inhibition efficiency decreased on the contrary. Futhermore, it would be quite useful to describe the adsorption process by an appropriate adsorption isotherm, which could provide further useful insights into the interaction of the inhibitor and the metal surface and on the mechanism of corrosion inhibition. Assuming that the surface coverage (θ) is proportional to the inhibition efficiency, data from Table 3 were used to determine the best adsorption isotherm. The considered adsorption isotherms including

- Frumkin isotherm $\frac{\theta}{1-\theta}\exp(-2f\theta) = K_{ads}C$
- Freundluich isotherm $\theta = K_{ads}C$
- Langmuir isotherm $\frac{\theta}{1-\theta} = K_{ads}C$
- Temkin isotherm $\exp(f\theta) = K_{ads}C$

where C is the inhibitor concentration, K_{ads} is the adsorption equilibrium constant, and f is the factor of energetic inhomogeneity. Ultimately, the best agreement was obtained with the Langmuir adsorption isotherm. Fig. 5 shows the data from Table 3 presented in the form of linearized Langmuir isotherm, $C/\theta = 1/K_{ads} + C$. When the degree of surface coverage (θ) tends to ~1, a more compact film is formed depending on the molecular structure of the compounds. The linear regression coefficient is almost equal to 1, indicating that HOBT molecules formed a single molecule adsorbed layer on the mild steel surface, and there was no interaction between adsorbed molecules.

Gibbs free energy (ΔG_{ads}) could be calculated with the following equation [39]:

$$\Delta G_{ads} = -RT\ln(55.5K_{ads}) \qquad (10)$$

where R is the gas constant, T is the temperature, the value 55.5 is the molecular concentration of water in solution in mol L^{-1}. In Fig. 5, the intercept on the vertical axis is the value of $1/K_{ads}$, which is 2.459×10^{-4}. Then according to Eq. (10), we calculated the $\Delta G_{ads} = -30.54$ kJ mol^{-1}. The quite negative value demonstrates that the HOBT adsorption process is highly spontaneous [40]. Besides, the absolute value of ΔG_{ads} is between 20 kJ mol^{-1} and 40 kJ mol^{-1}, so the adsorption of HOBT involves two types of interaction, chemisorption and physisorption.

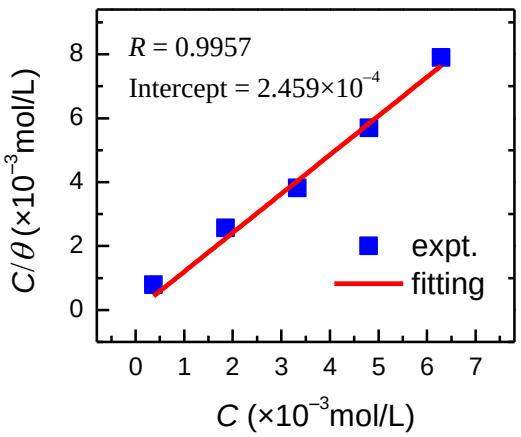

Figure 5. Langmuir adsorption isotherm of HOBT on the surface of mild steel.

3.4. SEM analysis

The surface morphology of mild steel samples immersed in 0.1 M H_2SO_4 solutions for 6 h at 298 K without and containing optimum concentration of HOBT was studied by SEM. As shown in Fig. 6, the steel sample before immersion seems smooth (Fig. 6a). In the absence of HOBT, the specimen surface is severely corroded, and the surface becomes porous and rough (Fig. 6b). In contrast, in the presence of HOBT, the surface of the specimen (Fig. 6c) is well protected. These results indicate that the corrosion of mild steel in 0.1 M H_2SO_4 solution is inhibited remarkably by HOBT.

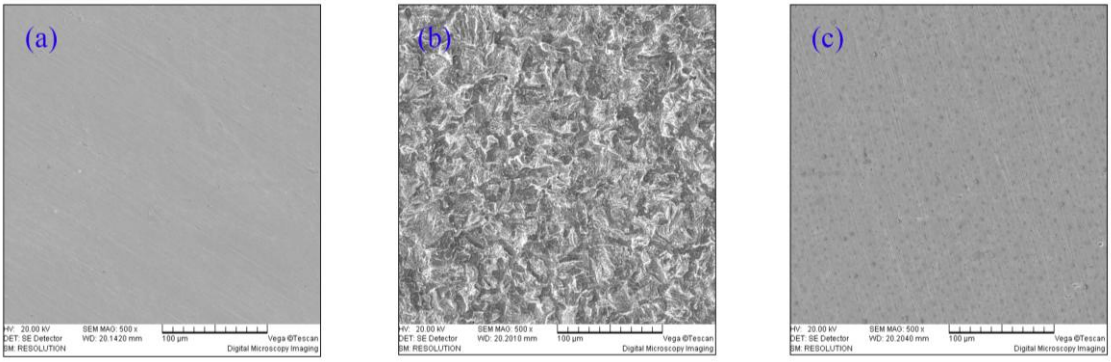

Figure 6. SEM micrographs of (a) freshly polished mild steel specimen and the specimens immersed in 0.1 M H_2SO_4 solution for 6 h without (b) and with 450 mg/L HOBT (c).

3.5. Theory study

The deprotonated form of HOBT stems from the following reaction in solution:

$$HOBT_{(aq)} \leftrightarrow OBT^{-}_{(aq)} + H^{+}_{(aq)} \qquad (11)$$

The pK_a constant for this reaction is 4.6 at 25 °C [41]. This implies that, at lower pH, the HOBT molecule is predominantly in neutral form, but as pH increases, the percentage of deprotonated molecules increases. For simplicity sake, we just consider the neutral molecule in the following discussions.

Frontier orbital theory was useful in predicting the adsorption centers of the inhibitor molecule responsible for the interaction with surface metal atoms [42]. It is generally acknowledged that in addition to HOMO and LUMO orbitals at least few other high lying occupied molecular orbitals (MO) should be considered to describe the molecule-surface bonding upon adsorption, since these MOs will probably hybridize with transition metal *d*-states [43]. In Fig. 7, four frontier occupied molecular orbitals HOMO−2, HOMO−1, HOMO and LUMO (where HOMO−*n* means *n*th MO below the HOMO) are provided. It can be seen from Fig. 7 that the HOMO−2 is of σ-type and is located on triazole ring, whereas the other three MOs are of π-type and are spread through the whole molecule. The HOMO−1 corresponds to *n*(N3) type lone-pair, whereas HOMO consists of *n*(N2, N4, N3, O) type lone-pair electrons; besides, both MOs display a π-type bonding on the benzene ring. On the other

hand, the LUMO orbitals, which can accept electrons from the metal using antibonding orbitals to form feedback bonds, are saturated around the rings and seemingly delocalized. In terms of the total electron density map (Fig. 8a), HOBT possesses electron rich property. As for the inhibitors in neutral forms, their adsorption geometry can be anticipated from the electrostatic potential plots presented in Fig. 8b–c. On this basis, it can be anticipated that HOBT would adsorb *via* N2 and N3 atoms.

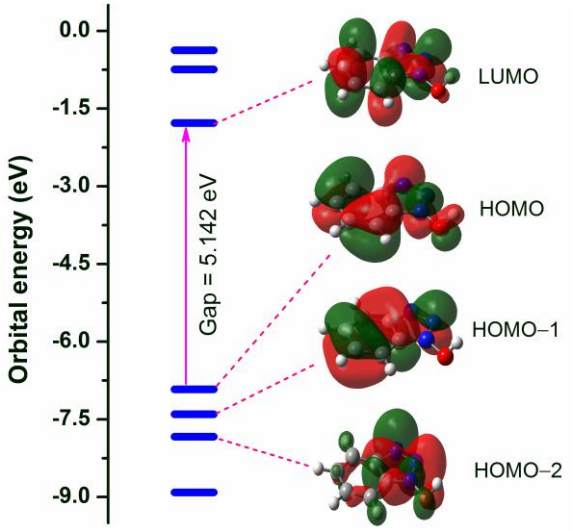

Figure 7. The frontier molecular orbitals of HOBT in particular HOMO–2, HOMO–1, HOMO and LUMO are plotted.

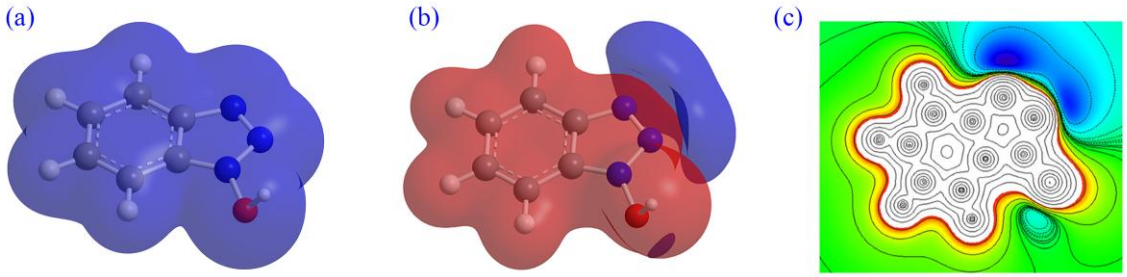

Figure 8. Electronic properties of HOBT: (a) total electron density, (b) Isosurface and (c) contour representation of electrostatic potential, respectively. Negative (positive) regions are colored blue (red).

To seek the most stable adsorption configuration, the adsorption behavior of HOBT on the Fe(110) surface have been investigated employing periodic slab models. Three stable adsorption configurations were identified and are shown in Fig. 9, together with their respective adsorption energies. Fig. 9a–b show the two configurations considered, one parallel to the surface and another one perpendicular to the iron surface. In the former case, a large structural distortion with some hydrogen atoms flipped up above the molecular cyclic skeleton is obtained, while the molecule is adsorbed on the Fe(110) surface in the bridging bidentate mode for the latter case. These two configurations are iso-

energetics at the DFT level (ΔE = 0.05 eV). However, the molecule would be oriented parallel (Fig. 9c) to the surface or nearly so to maximize its contact with the surface at the DFT-D level. The dispersion force's contributions to the adsorption energy is in the −0.2 ~ −0.3 eV range. This shows that at low coverage, dispersion represents about 10% of the total adsorption energy. The formation of the iono-covalent bond with the surface is the driving force for adsorption. Overall, the adsorption energies of all the adsorption configurations are more exothermic than presently reported adsorption energy for single water molecule on Fe(110) (*e.g.*, −0.26 eV) [44]. Actually, the adsorption of organic inhibitor molecules from the aqueous solution can be considered as a quasi-substitution process between the organic compounds in the aqueous phase [$Org_{(sol)}$] and water molecules associated with the metallic surface [$H_2O_{(ads)}$] as represented by the following equilibrium [45]:

$$Org_{(sol)} + xH_2O_{(ads)} \rightarrow Org_{(ads)} + xH_2O_{(sol)} \quad (8)$$

where x is the number of water molecules replaced by one organic molecule. Thus, the calculation results indicate that the water molecules can be easily substituted by HOBT adsorbate.

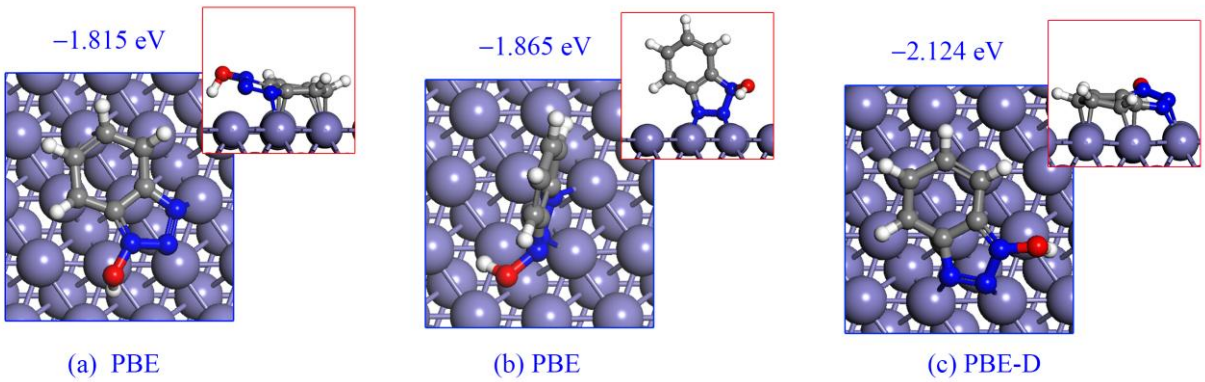

Figure 9. Three stable adsorption configurations (top view) of HOBT on Fe(110) surface together with their adsorption energies (insets: side view).

To gain some more insight into the chemistry of the iono-covalent bonds, we plot in Fig. 10 the density of states projected (PDOS) to the HOBT and to the Fe atoms in the first atomic layer of Fe(110). In all cases, 0 eV corresponds to the Fermi level. We can see that iron possesses open *d*-band, whicn can display strong chemisorption due to its large DOS at the E_F [46]. The purpose of Fig.10a is to show the alignment of the high-lying molecular valence states with the metal *d*-band before the interaction sets in. The HOMO is located 0.8 eV below the Fermi level (E_F), whereas LUMO is located almost 3 eV above the Fermi level. As mentioned before, there are several molecular states do lie at the position of the metal *d*-band. As demonstrated in Fig. 10b–c, the strong molecule-surface bonding is evident from the molecular PDOS, which is completely broadened due to a strong hybridization between molecular and metal states. The molecular PDOS is relatively unstructured in the vicinity of the Fermi energy for the parallel configuration. This behavior is different from the perpendicular adsorption configuration (Fig. 10c), in which the HOBT PDOSs show sharp peaks at the overlapping areas. The deformation electron density for both adsorption configurations are shown in Fig. 11. Red

and blue regions indicate the electron accumulation and depletion, respectively. We can see that the electron density is depleted from HOBT molecule, and accumulates on the Fe atoms (red area), which indicates the forming of the iono-covalent bonds. Hirshfeld charge analysis shows that the total charge of each adsorbed HOBT molecule is positive, and the values are 0.0149 *e* and 0.0325 *e* for the parallel and perpendicular adsorption configurations respectively. The large values of the adsorption energy are apparently a consequence of the strong interaction of the delocalized π-electrons of the aromatic rings (or nitrogen lone-pair orbitals of the triazole ring) with the surface Fe atoms.

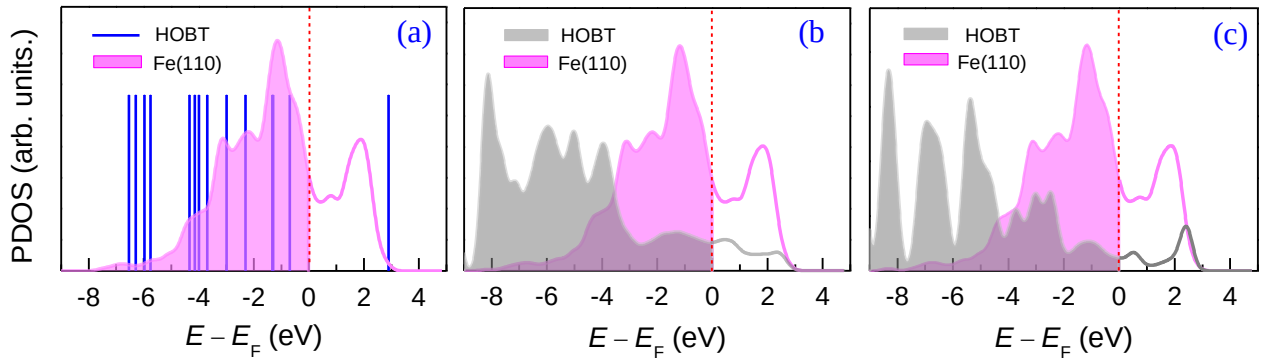

Figure 10. Density of states projected to HOBT and Fe atoms for (a) before the adsorption, (b) parallel and (c) perpendicular adsorption configurations.

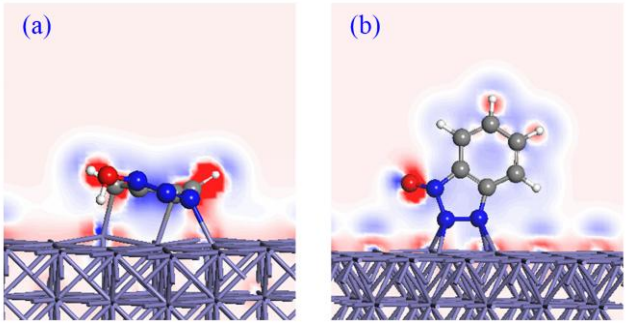

Figure 11. Deformation electron density for the (a) parallel and (b) perpendicular adsorption configurations.

3.6. Mechanism of adsorption and inhibition

A general mechanism for the dissolution of mild steel in H_2SO_4 solution would be similar to that reported in the literature [47]:

$$Fe + SO_4^{2-} \leftrightarrow (FeSO_4)_{ads} + 2e^- \quad (9)$$

$$(FeSO_4)_{ads} \leftrightarrow Fe(II) + SO_4^{2-} \quad (10)$$

However, for specimens in the inhibited H_2SO_4 solutions, the [Fe(0)HOBT] complex is formed at the flat area via the following reaction:

$$HOBT + Fe(0) \rightarrow [Fe(0)HOBT] \quad (11)$$

Schematic representation of the proposed mode of adsorption of HOBT molecule is shown in Fig. 12. It is shown that HOBT can react with Fe(0) and forms a complete protective film in the cathodic area. This film is very thin and is probably a single monolayer. Generally, in the corroded (*i.e.*, anodic area) area, SO_4^{2-} ions first adsorbed at the electrode/solution interface through electrostatic attraction force due to the excess positive charge at this interface. On the other hand, the HOBT molecule may exist either as protonated form (H_2OBT^+) or as neutral one in acid medium. Thus, the H_2OBT^+ may adsorb on iron surface through synergistic effect with sulfate radical and forms a thick and protective [Fe SO_4^{2-} H_2OBT^+] complex, by which, the metal surface is protected against being attacked by corrosive ions. It is important to note, however, H_2OBT^+ may be able to discharge in the metal surface that result in chemisorption [48]. Furthermore, the cathodic hydrogen evolution reaction may be given as follows [49]:

$$Fe + H^+ \leftrightarrow (FeH^+)_{ads} \quad (12)$$

$$(FeH^+)_{ads} + e^- \rightarrow (FeH)_{ads} \quad (13)$$

$$(FeH)_{ads} + H^+ + e^- \rightarrow Fe + H_2 \quad (14)$$

Then, the protonated HOBT molecules can be also adsorbed at cathodic sites of mild steel in competition with hydrogen ions that going to reduce to H_2 gas evolution.

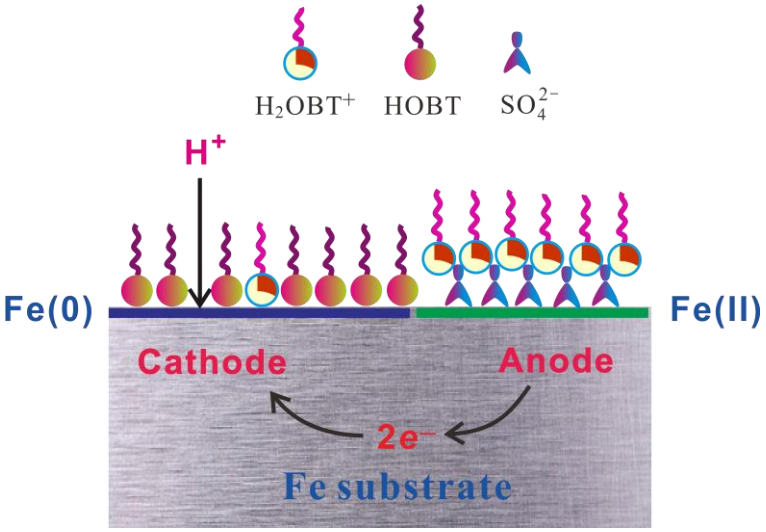

Figure 12. Proposed scheme for the adsorption of HOBT molecule on the iron surface in acid medium.

4. CONCLUSIONS

The following results can be drawn from this study:

- HOBT acts as a good inhibitor for the corrosion of mild steel in 0.1 M H_2SO_4 and its inhibition efficiency is concentration dependent.
- The polarization measurements reveal that HOBT behaves as a mixed-type inhibitor in

0.1 M H_2SO_4 by acting on both anodic metal dissolution and cathodic hydrogen evolution reactions.

- The adsorption of the inhibitor on the surface of mild steel in 0.1 M H_2SO_4 follows a Langmuir adsorption isotherm. The high value of adsorption equilibrium constant and negative value of standard free energy of adsorption suggested that HOBT is strongly adsorbed on mild steel surface.
- SEM micrographs show a smoother surface for inhibited metal samples than uninhibited samples due to the formation of a thin film.
- Several stable end configurations on the Fe(110) surface were theoretically identified for HOBT, with the parallel adsorption configuration (based on the DFT-D level) being the most stable.

ACKNOWLEDGEMENTS
This research was sponsored by the National Natural Science Foundation of China (21376282). We would like to thank the anonymous referees for valuable criticisms and useful suggestions that helped us to improve the quality of our present and future work.

References

1. M.M. Antonijevic, M.B. Petrovic, *Int. J. Electrochem. Sci.*, 3 (2008) 1.
2. M. Finsgar, I. Milosev, *Corros. Sci.*, 52 (2010) 2737.
3. B.E.A. Rani, B.B.J. Basu, *Int. J. Corros.*, 2012 (2012) 1.
4. G. Gece, *Corros. Sci.*, 50 (2008) 2981.
5. S.M.A. Hosseini, M. Salari, M. Ghasemi, *Mater. Corros.*, 60 (2009) 963.
6. S.T. Zhang, Z.H. Tao, S.G. Liao, F.J. Wu, *Corros. Sci.*, 52 (2010) 3126.
7. H.L. Wang, H.B. Fan, H.S. Zheng, *Mater. Chem. Phys.*, 77 (2003) 655.
8. M.K. Awad, R.M. Issa, F.M. Atlam, *Mater. Corros.*, 60 (2009) 813.
9. M.L. Zheludkevich, K.A. Yasakau, S.K. Poznyak, M.G.S. Ferreira, *Corros. Sci.*, 47 (2005) 3368.
10. M. Finsgar, J. Kovac, I. Milosev, *J. Electrochem. Soc.*, 157 (2010) C52.
11. M. Finsgar, A. Lesar, A. Kokalj, I. Milosev, *Electrochim. Acta*, 53 (2008) 8287.
12. L. Tommesani, G. Brunoro, A. Frignani, C. Monticelli, M. DalColle, *Corros. Sci.*, 39 (1997) 1221.
13. K.F. Khaled, *Mater. Chem. Phys.*, 112 (2008) 290.
14. K. Babic-Samardzija, N. Hackerman, *J. Solid State Electrochem.*, 9 (2005) 483.
15. A. Kokalj, S. Peljhan, *Langmuir*, 26 (2010) 14582.
16. J.O. Mendes, E.C. da Silva, A.B. Rocha, *Corros. Sci.*, 57 (2012) 254.
17. J.H. Xu, W.H. Hu, *Chin. J. Chem. Phys.*, 16 (2003) 189.
18. D. Costa, P.A. Garrain, B. Diawara, P. Marcus, *Langmuir*, 27 (2011) 2747.
19. M. Sacchi, S.J. Jenkins, *Phys. Chem. Chem. Phys.*, 16 (2014) 6101.
20. W. Reckien, F. Janetzko, M.F. Peintinger, T. Bredow, *J. Comput. Chem.*, 33 (2012) 2023.
21. C.T. Lee, W.T. Yang, R.G. Parr, *Phys. Rev. B*, 37 (1988) 785.
22. J.P. Perdew, K. Burke, M. Ernzerhof, *Phys. Rev. Lett.*, 78 (1997) 1396.
23. B. Delley, *Phys. Rev. B*, 66 (2002) 155125.
24. B. Delley, *J. Chem. Phys.*, 113 (2000) 7756.
25. J.R. Mohallem, T.D. Coura, L.G. Diniz, G. de Castro, D. Assafrao, T. Heine, *J. Phys. Chem. A*, 112 (2008) 8896.
26. R.L. Camacho-Mendoza, E. Aquino-Torres, J. Cruz-Borbolla, J.G. Alvarado-Rodríguez, O. Olvera-Neria, J. Narayanan, T. Pandiyan, *Struct. Chem.*, 25 (2014) 115.
27. E.P. Yelsukov, E.V. Voronina, V.A. Barinov, *J. Magn. Magn. Mater.*, 115 (1992) 271.

28. G. Autès, C. Barreteau, D. Spanjaard, M.-C. Desjonquères, *J. Phys.: Condens. Matter*, 18 (2006) 6785.
29. R. Soulairol, C.C. Fu, C. Barreteau, *J. Phys.: Condens. Matter*, 22 (2010) 295502.
30. S. Grimme, *J. Comput. Chem.*, 27 (2006) 1787.
31. E.S. Ferreira, C. Giacomelli, F.C. Giacomelli, A. Spinelli, *Mater. Chem. Phys.*, 83 (2004) 129.
32. A.O. Yuce, G. Kardas, *Corros. Sci.*, 58 (2012) 86.
33. M. Gholami, I. Danaee, M.H. Maddahy, M. RashyandAvei, *Ind. Eng, Chem, Res.*, 52 (2013) 14875.
34. E.M. Sherif, S.M. Park, *Electrochim. Acta*, 51 (2006) 1313.
35. A. Zarrouk, B. Hammouti, H. Zarrok, M. Bouachrine, K.F. Khaled, S.S. Al-Deyab, *Int. J. Electrochem. Sci.*, 7 (2012) 89.
36. M. Ozcan, F. Karadag, I. Dehri, *Colloids Surf., A*, 316 (2008) 55.
37. M. Hosseini, S.F.L. Mertens, M. Ghorbani, M.R. Arshadi, *Mater. Chem. Phys.*, 78 (2003) 800.
38. H.H. Hassan, *Electrochim. Acta*, 51 (2006) 5966.
39. D.W. Vankrevelen, H.A.G. Chermin, *Chem. Eng. Sci.*, 1 (1951) 66.
40. S. Ghareba, S. Omanovic, *Electrochim. Acta*, 56 (2011) 3890.
41. R. Subiros-Funosas, A. El-Faham, F. Albericio, *Org. Biomol. Chem.*, 8 (2010) 3665.
42. S. John, A. Joseph, *Mater. Corros.*, 64 (2013) 625.
43. N. Kovacevic, A. Kokalj, *Corros. Sci.*, 53 (2011) 909.
44. M. Eder, K. Terakura, J. Hafner, *Phys. Rev. B*, 64 (2001).
45. A.U. Ezeoke, O.G. Adeyemi, O.A. Akerele, N.O. Obi-Egbedi, *Int. J. Electrochem. Sci.*, 7 (2012) 534.
46. N. Kovacevic, A. Kokalj, *Mater. Chem. Phys.*, 137 (2012) 331.
47. A. Doner, R. Solmaz, M. Ozcan, G. Kardas, *Corros. Sci.*, 53 (2011) 2902.
48. A. Kokalj, *Corros. Sci.*, 68 (2013) 195.
49. S. John, B. Joseph, K.K. Aravindakshan, A. Joseph, *Mater. Chem. Phys.*, 122 (2010) 374.